


Pedometric tools for classification of southwestern Amazonian soils: A quali-quantitative interpretation incorporating visible-near infrared spectroscopy

Journal of Near Infrared Spectroscopy
2022, Vol. 0(0) 1–13
© The Author(s) 2022
Article reuse guidelines:
sagepub.com/journals-permissions
DOI: 10.1177/09670335211061854
journals.sagepub.com/home/jns


Orlando CH Tavares¹, Tiago R Tavares², Carlos R Pinheiro Junior¹, Luciélío M da Silva³, Paulo GS Wadt⁴ and Marcos G Pereira¹ 

Abstract

The southwestern region of the Amazon has great environmental variability, presents a great complexity of pedoenvironments due to its rich variability of geological and geomorphological environments, as well as for being a transition region with other two Brazilian biomes. In this study, the use of pedometric tools (the Algorithms for Quantitative Pedology (AQP) R package and diffuse reflectance spectroscopy) was evaluated for the characterization of 15 soil profiles in southwestern Amazon. The AQP statistical package—which evaluates the soil in-depth based on slicing functions—indicated a wide range of variation in soil attributes, especially in the superficial horizons. In addition, the results obtained in the similarity analysis corroborated with the description of physical, chemical components and oxide contents in-depth, aiding the classification of soil profiles. The in-depth characterization of visible-near infrared spectra allowed inference of the pedogenetic processes of some profiles, setting precedents for future work aiming to establish analytical strategies for soil classification in southwestern Amazon based on spectral data.

Keywords

Pedometrics, AQP R package, soil-depth functions, soil attributes, diffuse reflectance spectroscopy

Received 22 April 2021; accepted 7 November 2021

Introduction

The state of Rondônia is located in the southwestern portion of the Amazon and occupies an area of 237,765.347 km² ($\pm 4.7\%$ of Brazilian Amazon biome) (IBGE 2021), constituting part of its southern boundary with the formations of Central Brazil.¹ It is a region of transition between three of the six Brazilian terrestrial biomes: Amazon, Cerrado, and Pantanal.² In addition to the high variability of plant physiognomy,^{1,3} this region is also characterized by a great geological and geomorphological diversity. The landscape oscillates from river plains, flattened surfaces, and depressions to dissected and sedimentary tablelands and plateaus.^{4,5} These characteristics promote a complex diversity of pedoenvironments in this region, with great variability of soil classes (e.g., Ferralsols, Lixisols, Acrisols, Arenosols, Regosols, Leptosols, Fluvisols, Plinthosols, among others).^{4,6} The most predominant soils are Acrisols (39.12%) followed by Ferralsols (36.31%), Arenosols (5.96%), and Plinthosols (4.50%).⁷

The classification of soils by traditional methods that involve morphological and pedogenetic description, in addition to the quantification and interpretation of chemical, physical, and molecular attributes, is a challenge, given the complexity of these data analyses. For the classification of a

reasonable amount of soil profiles, it is necessary to synthesize information on chemical attributes, soil depth, and horizon thicknesses, which in most cases requires experienced professional for data interpretation and correct classification. However, the use of quantitative analysis for soil classification can facilitate the interpretation and visualization of the variability of soil attributes, being a useful strategy to analyze the large volume of information generated from soil profiles.⁸ To meet this demand, the Algorithms for Quantitative Pedology (AQP) package has been developed and implemented in R software.⁹ This package makes it

¹Departamento de Solos, Universidade Federal Rural do Rio de Janeiro (UFRRJ), Seropédica, Brazil

²Centro de Energia Nuclear na Agricultura (CENA) da Universidade de São Paulo (USP), Piracicaba, Brazil

³Empresa Brasileira de Pesquisa Agropecuária—Embrapa Acre, Rio Branco, Brazil

⁴Empresa Brasileira de Pesquisa Agropecuária (Embrapa Agroflorestal), Porto Velho, Brazil

Corresponding author:

Marcos G Pereira, Departamento de Solos, Universidade Federal Rural do Rio de Janeiro (UFRRJ), BR 465 km 7, Seropédica 23890-000, Brazil.
Email: mgervasiopereira01@gmail.com

possible to make standard profile sketches to highlight differences in soil attributes between horizons. In addition, this package also features a slicing algorithm (called slice-wise algorithm) that allows harmonization of soil profile data and analysis of similarity between different profiles.^{9–11}

Another problem associated with studies of soil profile collections is the large volume of soil samples to be analyzed physically and chemically. As an alternative to traditional laboratory methods, diffuse reflectance spectroscopy in the visible (vis; 400–700 nm) and near infrared (NIR; 700–2500 nm) ranges has been widely used for predicting soil attributes in different regions of the world,^{12–15} allowing faster, cheaper analyses with no use of chemical reagents.^{16–19}

Interpretation of the visible-near infrared (vis-NIR) spectra by chemometric tools enables qualitative and quantitative evaluations of morphological, physical, and chemical attributes of the soil, such as color, organic carbon content, mineralogy, degree of crystallinity of iron oxides, clay content and textural classes, in addition to inferences on the action of pedogenetic processes.^{17–24} The attributes mentioned above are used as diagnostic characteristics in soil classification systems,^{25,26} which makes vis-NIR spectroscopy promising for classification of soil profiles.^{27–31}

However, for a more precise and detailed use of soil attributes for classification purposes, it is necessary to evaluate the spectra of each horizon of the profile, seeking to better understand its variation in subsurface. On the other hand, the adoption of this method may result in a large volume of information, especially in studies with soil profile collections, making it difficult to interpret the results. In this context, the application of soil-depth functions, harmonization, and interpolation of the data, as well as the schematic sketches generated by the AQP package, facilitates the visualization of the variability of soil attributes in subsurface and can help to interpret the vis-NIR spectra of the horizons.

In view of the above, the aim of this study was to evaluate the use of the AQP package for the characterization of physical and chemical attributes and comparison of soil profiles. In addition, the schematic sketches created by the

AQP package were compared with the behavior of the vis-NIR spectra of the soil profiles, seeking to provide basis for future applications of these pedometric tools for the classification of soils in the southwestern Amazon.

Material and methods

Study areas and characterization of samples via traditional methods

Morphological, physical, and chemical data of 106 samples from 15 soil profiles (one per horizon) were used. The profiles are located under different pedoenvironmental conditions, 14 profiles in the State of Rondônia and one in the State of Amazonas, Northern Region of Brazil (Figure 1). Morphological description of the soil profiles and disturbed samples for physical and chemical analyses were collected from all horizons according to Santos et al. (2015). The region has a great geological diversity, where metamorphic rocks such as gneiss, sedimentary rocks such as claystones and sandstones, and sediments of Holocene and Pleistocene age can be observed.³² The relief and landscape that the profiles are inserted, the specific location of each soil profile and its classification by both the Brazilian Soil Classification System²⁶ and the World Reference Base for Soil Resources (WRB)²⁵ are presented in the Table 1.

Physical and chemical analyses were performed according to Empresa Brasileira DE Pesquisa Agropecuária (EMBRAPA),³³ as described by Lumberras et al,³² quantifying the particle-size fractions (Table 2), coarse sand (CS), fine sand (FS), total sand (TS), Silt, Clay, flocculation degree (FD), silt/clay, particle density (PD), color; and the chemical attributes (Table 2), ΔpH ($\text{pH}_{\text{KCl}} - \text{pH}_{\text{H}_2\text{O}}$), $\text{Ca}^{2+} + \text{Mg}^{2+}$, K^+ , Na^+ , sum of bases (SB), Al^{3+} , H^+ , cation exchange capacity (CEC), base saturation (V), aluminum saturation (m), P, soil organic carbon (SOC) (Nelson and Sommers),³⁴ and soil total nitrogen (STN). The contents of oxides (chemical composition of important clay mineral groups), SiO_2 ,

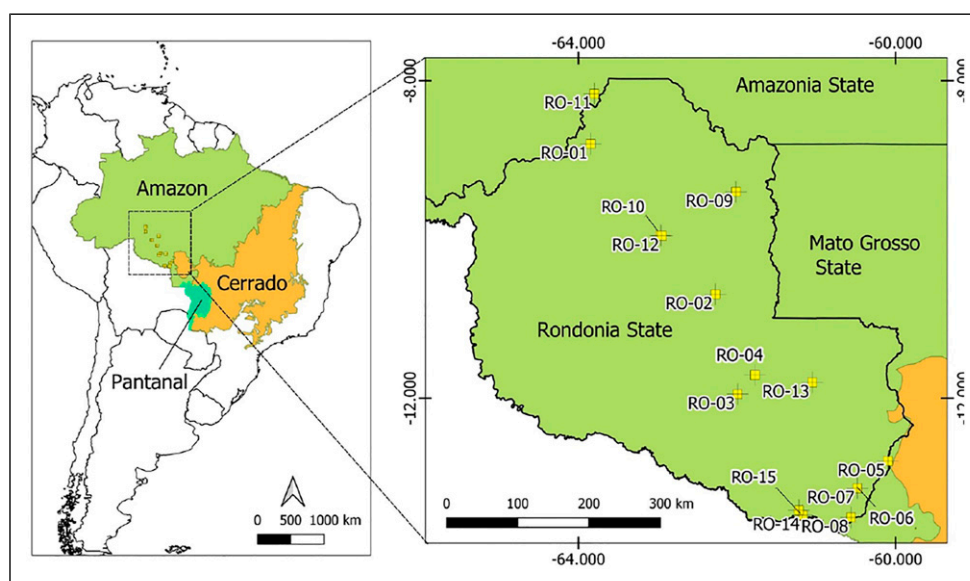


Figure 1. Location of the study area and distribution of the soil profiles collected.

Table 1. Location and classification of the studied soil profiles.

| Profile | Coordinates | Relief | Landscape | SiBCS ⁽¹⁾ | WRB ⁽²⁾ | Abbreviation - WRB |
|---------|------------------------------------|---|------------------------------------|--|---|------------------------|
| RO-01 | 08° 47' 46.3" S 63° 50' 46.5" W | Flat | Quicuiu grass pasture | Plintossolo Háplico Distrófico típico | Katostagnic Plinthosol (Endoacric, Hyperdystric, Ochric, Anosiltic, Bathyclayic) | Katostagnic PT-RO.01 |
| RO-02 | 10° 41' 20.2" S 62° 16' 22.3" W | Smooth rolling | Pasture | Argissolo Vermelho-Amarelo Eutrófico típico | Katolixic Ferralsol (Katoclayic, Hypereutric, Epiloamic, Ochric Katovetic) | Katolixic FR-RO.02 |
| RO-03 | 11° 56' 53.3" S 61° 59' 34.6" W | Smooth rolling | Pasture | Nitossolo Vermelho Eutroférico típico | Hypereutric Katolixic Katosideralic Nitisol (Ochric, Bathyvertic) | Katosideralic NT-RO.03 |
| RO-04 | 11° 42' 16.6" S 61° 46' 31.0" W | Flat | Orchard of fruit trees and grasses | Cambissolo Háplico Tb Distrófico saprolítico gleissólico petroplintico | Endodystric Epieutric Episkeletic Regosol (Epigeoabruptic, Loamic Magnesic, Ochric, Amphiraptic, Bathyrelictistagnic, Amphiferric) | Episkeletic RG-RO.04 |
| RO-05 | 12° 47' 27.3" S 60° 06' 2.6" W | Plateau and flat | Grasses | Latossolo Vermelho-Amarelo Ácrico típico | Geric Ferralsol (Pantoclayic, Oligoeutric, Humic) | Geric FR-RO.05 |
| RO-06 | 13° 08' 02.3" S 60° 29' 02.5" W | Lower third of slope with 6–8% slope | Forage grasses | Argissolo Vermelho-Amarelo Eutrófico luvisólico | Chromic Epiabruptic Lixisol (Amphiclayic, Cutanic, Loamic, Ochric Epiraptic) | Epiabruptic LX-RO.06 |
| RO-07 | 13° 07' 56.5" S 60° 29' 08.0" W | Terrace with 1 to 3% slope | Forage grasses | Gleissolo Háplico Tb Distrófico planossólico | Endodystric Epieutric Endoacric Amphialbic Stagnosol (Endoclayic Katoferralic, Anoloamic, Ochric) | Amphialbic ST-RO.07 |
| RO-08 | 13° 30' 0.9" S 60° 33' 42.1" W | Middle third to lower third of slope (about 800 m) with 2 to 3% slope | Pasture | Argissolo Vermelho Eutrófico abruptico latossólico antrópico | Lixic pretic Rhodic Ferralsol (Katoclayic, Hypereutric, Humic, Epiloamic, Bathypisoplinthic) | Rhodic FR-RO.08 |
| RO-09 | 09° 23' 59.3" S 62° 00' 58.9" W | Flat | Grasses | Latossolo Amarelo Ácrico típico | Geric Xanthic Ferralsol (Pantoclayic, Orthodystric, Ochric) | Xanthic FR-RO.09 |
| RO-10 | 09° 56' 54.2" S 62° 57' 57.7" W | Elevation top with 0–1% slope | Secondary forest | Latossolo Vermelho-Amarelo Distrófico típico | Haplic Ferralsol (Pantoclayic, Oligoeutric, Humic, Pantovetic) | Haplic FR-RO.10 |
| RO-11 | 08° 09' 47.2" S 63° 48' 04.6" W | Flat | Forage grasses | Plintossolo Argilúvico Alumínico gleissólico | Amphialbic Katostagnic Plinthosol (Endoacric, Hyperdystric Amphiloamic, Ochric, Bathyclayic) | Katostagnic PT-RO.11 |
| RO-12 | 09° 57' 10.0" S 62° 56' 51.4" W | Third higher than middle third with 3–5% slope | Forage grasses | Latossolo Amarelo Distrófico típico | Xanthic Ferralsol (Pantoclayic, Oligoeutric, Humic, Endoraptic, Katovetic) | Xanthic FR-RO.12 |
| RO-13 | 11° 47' 56.5" S 61° 03' 11.6" W | Plateau (interfluvium with 1–2% slope) | Cerrado vegetation | Cambissolo Háplico Ta Eutrófico saprolítico vertissólico epiirredóxico | Hypereutric Katostagnic Gleysol (Anoclayic, Ochric, Endoraptic, Uterquic, Amphiprotovetic, Magnesic) | Katostagnic GL-RO.13 |
| RO-14 | 13° 28' 26.0" S 61° 10' 30.9" W | Terrace on the plain of the Guaporé with 0–1% slope | Pasture | Latossolo Amarelo Distrófico petroplintico plintossólico | Umbric Ferralsol (Endoclayic, Hyperdystric, Endoferric, Anoloamic, Endostagnic, Endovetic) | Umbric FR-RO.14 |
| RO-15 | 13° 24' 36.8" S 61° 13' 15.0" W | Terrace on the plain of the Guaporé with 0–1% slope | Natural field | Plintossolo Háplico Ácrico gleissólico petroplintico húmico | Geric umbric Ferralsol (Oligoeutric, Endoferric, Humic, Pantoloamic, Katostagnic) | Umbric FR-RO.15 |

Legend: (1) SiBCS = Brazilian Soil Classification System; (2) WRB = World Reference Base for Soil Resources.

Al₂O₃, Fe₂O₃, TiO₂, P₂O₅, and MnO, were also quantified by sulfuric attack³⁵ and were used to calculate the weathering indices Ki [(SiO₂/Al₂O₃)×1.7] and Kr {(SiO₂/0.6)/[(Al₂O₃/1.02)+(Fe₂O₃/1.60)]} and Al₂O₃/Fe₂O₃ ratio (Table 2).

Aggregation of soil horizons by depth slices

Numerical models were created to describe the variability in subsurface of physical attributes, chemical attributes, and oxide contents in each profile (Table 2). This procedure was

Table 2. Physical, chemical, and oxides (chemical composition of important clay mineral groups) attributes and molecular ratio properties of the complete set of soils from the State of Rondônia, Brazil.

| Physical attributes | Units | Chemical attributes | units | Oxide attributes | units |
|---------------------|--------------------|------------------------------------|------------------------------------|--|--------------------|
| CS | g kg ⁻¹ | ΔpH | — | SiO ₂ | g kg ⁻¹ |
| FS | g kg ⁻¹ | Ca ²⁺ +Mg ²⁺ | cmol _c kg ⁻¹ | Al ₂ O ₃ | g kg ⁻¹ |
| TS | g kg ⁻¹ | K ⁺ | cmol _c kg ⁻¹ | Fe ₂ O ₃ | g kg ⁻¹ |
| Silt | g kg ⁻¹ | Na ⁺ | cmol _c kg ⁻¹ | TiO ₂ | g kg ⁻¹ |
| Clay | g kg ⁻¹ | SB | cmol _c kg ⁻¹ | P ₂ O ₅ | g kg ⁻¹ |
| FD | % | Al ³⁺ | cmol _c kg ⁻¹ | MnO | g kg ⁻¹ |
| Silt/Clay | — | H ⁺ | cmol _c kg ⁻¹ | Ki | — |
| PD | Mg m ⁻³ | H ⁺ +Al ³⁺ | cmol _c kg ⁻¹ | Kr | — |
| hue | — | CEC | cmol _c kg ⁻¹ | Al ₂ O ₃ /Fe ₂ O ₃ | — |
| value | — | V | % | | |
| chroma | — | m | % | | |
| | | P | mg kg ⁻¹ | | |
| | | SOC | g kg ⁻¹ | | |
| | | STN | g kg ⁻¹ | | |

CS = coarse sand; FS = fine sand; TS = total sand; FD = flocculation degree; PD = particle density; SB = sum of bases; CEC = cation exchange capacity; V = base saturation; m = aluminium saturation; SOC = soil organic carbon; STN = soil total nitrogen; Ki = $[(\text{SiO}_2/\text{Al}_2\text{O}_3) \times 1.7]$; Kr = $\{(\text{SiO}_2/0.6)/[(\text{Al}_2\text{O}_3/1.02) + (\text{Fe}_2\text{O}_3/1.60)]\}$.

performed using the slice-wise algorithm,⁹ which uses the soil profiles database to model the behavior of its attributes in subsurface, creating a soil-depth function.

Numerical classification of soil profiles

From the database generated for 1-cm-thick layers, the dissimilarity matrix between the profiles was calculated, allowing the evaluation of similarity.⁹ The dissimilarity between the studied soils was calculated using the “profile compare” function, based on the comparison of the abovementioned oxides, physical, and chemical attributes, considering the maximum depth and weighting coefficient equal to 0.01. The number of profiles used in the calculation is represented by the contribution fraction, whose value can be considered as an aggregate measure of probability for each depth of the soil. Additionally, a function was used to render the schemes of the profiles, according to the soils. The algorithm is useful for standardizing the visualization of soil profile sketches, allowing analyses and comparisons for taxonomic and/or utilitarian purposes.^{9,11} All statistical procedures and application of soil-depth functions were performed using the AQP package,⁹ using R software.³⁶

Acquisition and analysis of vis-NIR spectra

The NIRS™ DS2500 spectrometer (FOSS, Hillerød, Denmark) was used to acquire vis-NIR spectra from 400 to 2500 nm, with spectral resolution of 1 nm. Before spectral acquisition, the spectrometer was calibrated using standard white plate, repeating this procedure every 20 samples. Spectral analyses were performed in dry samples, with particle-size of less than 2 mm, following the preparation of samples adopted by the Spectral Soil Library of Brazil.³⁷ Three spectral readings were applied at different positions of the sample surface in order to consider the analytes micro-heterogeneity, and then the mean of the spectra was obtained for the following analyses. All measurements were made under a controlled environment (laboratory).

To assist in understanding the response of the spectra in relation to the different characteristics of the soil profiles, spectra of each profile were subjected to descriptive analysis in order to characterize the intensity, shape, and absorption features present in the spectral curves.³⁸

Results and discussion

Physical, chemical, and oxide attributes

The vertical variability of soil attributes tends to be continuous in a soil profile and, for this reason, soil-depth functions are usually used to represent this perspective of the profile.^{11,39–41} The functions for representing the particle-size, chemical, and oxide compositions in subsurface of the set of soil profiles are presented in Figure 2. The percentage values plotted (to the right of each chart) along the profile show the relative number of profiles used in the soil-depth function to calculate the statistics (median and quartiles, with distribution between 25 and 75 percentiles) for each depth. The contribution of 100% of the profiles used in the calculation extends up to approximately 1.25 m deep, although up to 1.50 m deep there is a contribution of 87% of the profiles to all attributes (Figure 2).

The total sand and fine sand contents decrease in subsurface with high variability around the median value, with a behavior generally inverse to that of clay content throughout the profile (Figure 2A). These results are consistent with those found by Pinheiro et al.⁴² especially when peaks occur in the curves, especially of 50–175 cm (probably related to transitions between horizons, and/or the presence of diagnostic horizons).

The clay content ranges from about 200 to 500 g kg⁻¹ near the surface, increasing linearly up to about 60 cm and approaches a median value of the entire collection of about 400 g kg⁻¹ (Figure 2A). The variability in clay content is lower near the surface and usually increases in subsurface, reaching 700 g kg⁻¹ at 175 cm. As for silt contents, it is possible to observe a reduction in the median value up to

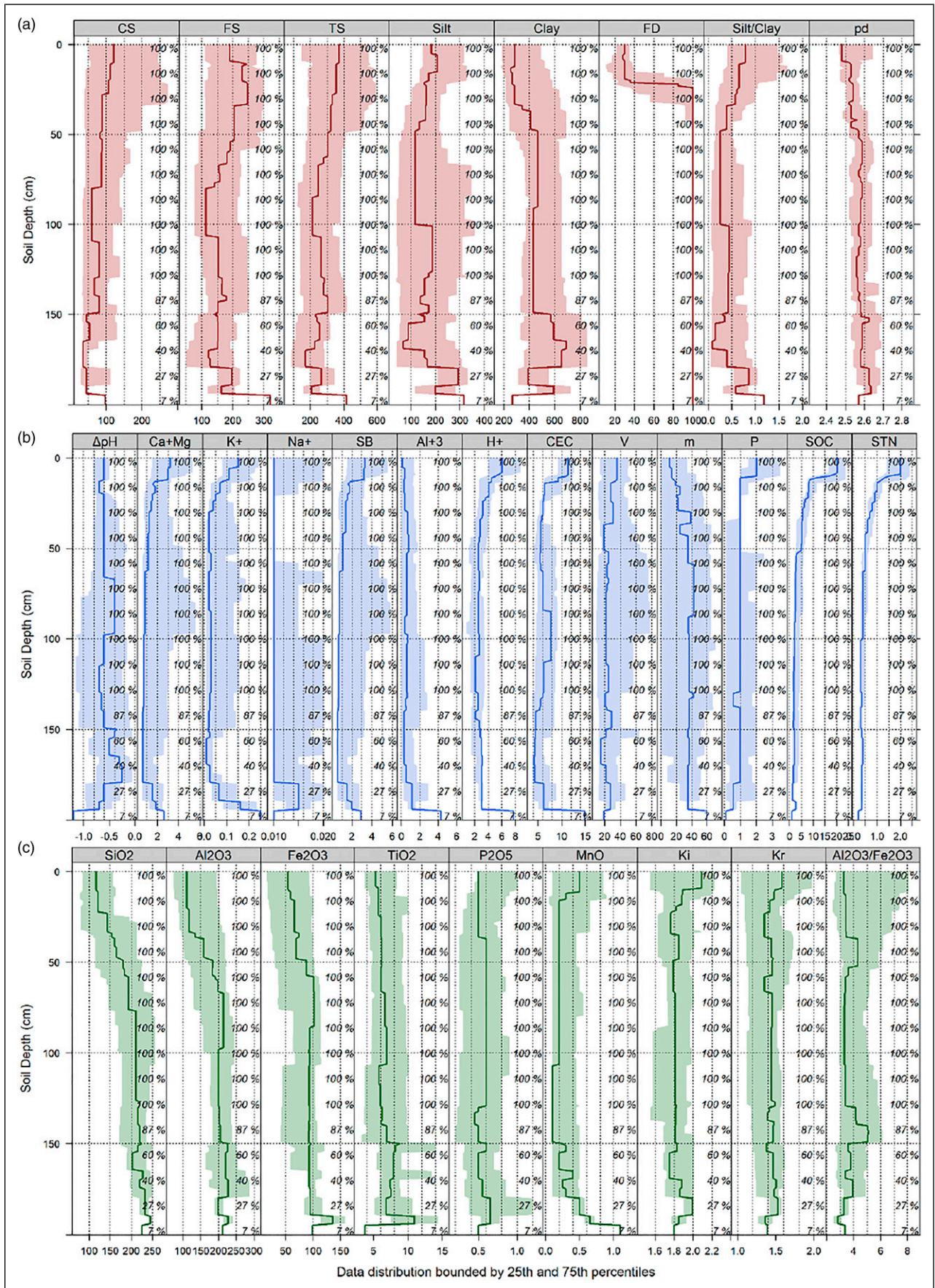


Figure 2. Soil-depth functions to represent the vertical variability from the State of Rondônia, Brazil. Medians of physical (A), chemical (B), and oxide (chemical composition of important clay mineral groups) attributes and molecular ratio properties (C) from the complete set of soils. CS, FS, TS = coarse, fine, and total sand, FD = flocculation degree, PD = particle density, SB = sum of bases, CEC = cation exchange capacity, V = base saturation, m = aluminum saturation, SOC= soil organic carbon, STN= soil total nitrogen. The medians are represented by the red, blue, and green lines and bounded by the 25th and 75th percentiles.

100 cm, with high variability up to 150 cm depth, followed by increments of two times in its content.

It was observed that the attributes showed a continuous trend along the depth, with greater variability for the particle-size composition and lower variability for the flocculation degree (FD) and particle density (PD) (Figure 2A). FD varies up to 0.50 m, with values below 40% in surface and of 100% from 0.25 m onward. This is probably due to the smaller contribution of organic matter in the deeper layer than in the surface, since the surface is more benefited by organic matter from the deposition of plant residues.⁴³ The dispersion–flocculation phenomenon is influenced by soil organic matter,⁴⁴ which affects the development of the structure and is related to the balance of electrical charges in the soil.⁴⁵ The high FD found in most horizons is coherent for the class of Ferralsols, which are usually associated with values close to 100%.

Most chemical attributes decrease linearly up to about 170 cm and others such as $\text{Ca}^{2+}+\text{Mg}^{2+}$, K^+ , SB, and CEC increase after that point (Figure 2B). On the other hand, the variability of ΔpH , $\text{Ca}^{2+}+\text{Mg}^{2+}$, K^+ , Na^+ , SB, V, and P is lower near the surface and usually increases in subsurface (Figure 2B). The values of sum of basis (SB) and cation exchange capacity (CEC) followed the distribution of the $\text{Ca}^{2+}+\text{Mg}^{2+}$ ions, the predominant cations in the soils. Similar results were observed for vertical variability in-depth in Amazonian Dark Earths soils in Rondônia State.⁴⁶ However, contrary to the results of this study, the variation and depth of the contents of Ca^{2+} , K^+ , and Na^+ increase in-depth in soils from a Brazilian semi-arid environment.¹¹

It was possible to observe that the median values of SOC and STN, represented by the soil-depth function, tend to decrease from 20 cm, as observed for SOC by Minasny et al.,⁴⁷ with a zone of greater variability between 0 and 20 cm (Figure 2B), and for H^+ and CEC the values decrease from 50 cm (Figure 2B). The aggregate trend in SOC and STN in subsurface follows the typical exponential decay curve.⁹ The most widely used model for soil-depth functions is the exponential or power model, which is mainly used to describe soil organic matter distribution or organic carbon content in subsurface. The function describes the decrease of soil organic matter or total carbon and nitrogen in subsurface (higher in the A horizon and lower in the subsequent horizons),⁴⁷ as well as for H^+ , CEC, and P, a pattern verified in this study (Figure 2B).

With the exception of the RO-13 profile, the soils are deep with horizons extending to depths greater than 150 cm. The variability in SiO_2 , Al_2O_3 , and Fe_2O_3 contents is lower in surface and generally increases in subsurface. SiO_2 content ranges from about 100 to 150 g kg^{-1} near the surface, and the median increases linearly up to about 150 cm and approaches a median value of the entire collection of about 200 g kg^{-1} , reaching 250 g kg^{-1} at 200 cm (Figure 2C). Al_2O_3 content ranges from about 100 to 250 g kg^{-1} in surface, increases linearly up to about 100 cm, and approaches a median value of about 200 g kg^{-1} . Fe_2O_3 content ranges from about 5 to 100 g kg^{-1} in surface, increases linearly to about 75 cm, and approaches a median value of about 100 g kg^{-1} (Figure 2C).

The median contents of TiO_2 and P_2O_5 virtually do not vary in subsurface, but the content of MnO decreases in

surface and increases from 150 cm. The median values of Ki and Kr decrease near the surface and remain constant in subsurface horizons (Figure 2C). However, the variability of the $\text{Al}_2\text{O}_3/\text{Fe}_2\text{O}_3$ ratio is high near the surface and decreases in subsurface horizons, with little variation of the median.

Despite the similar behavior of some of the evaluated attributes, in general, a great variability is observed, which may be related to the geological diversity of the region³² and the intense dynamics of pedogenesis in tropical environments. Due to this, other analysis tools are necessary for a better characterization and comparison of the particle-size,¹⁰ chemical, and oxide composition of these profiles. SB, CEC, SOC, clay content, Fe_2O_3 , and Ki per horizon of each of the soil profiles were selected (Figure 3).

Standardized sketches for representation of soil profiles are useful for pedologists, since they portray the stratigraphy of horizons and their transitions.⁹ The visualization of the sketches makes it possible to highlight predominance in the particle-size, chemical, and oxide compositions, as observed for the horizons of the different soil orders of the State of Rondônia (Figure 3), and also verified for the particle-size in studies of hydromorphic soils,¹⁰ Ferralsols,⁴² and collection of soil profiles of the Brazilian semi-arid region.¹¹ Thus, the particle-size analysis showed higher values for clay in the Ferralsols, in surface and subsurface; in addition, these soils have higher clay content than those presented by Pinheiro et al.⁴²

The highest SB contents throughout the profile were observed in Rhodic FR, followed by Hypereutric Katostagnic Gleysol, Katosideralic Nitisol, and Katolixic Ferralsol (Figure 3A). On the other hand, the Umbric Ferralsol, followed by the Amphialbic Katostagnic Plinthosol and Katostagnic Plinthosol had lower SB (Figure 3A).

The values of CEC (15 $\text{cmol}_c \text{ kg}^{-1}$) in Geric Umbric Ferralsol and Ferralsols, especially Geric Ferralsol, were the lowest ones (Figure 3B). On the other hand, Hypereutric Katostagnic Gleysol showed high values of CEC, which reached 25 $\text{cmol}_c \text{ kg}^{-1}$.

However, the CEC values in Geric Umbric Ferralsol and Ferralsols, especially Geric Ferralsol, were the lowest ones (Figure 3B), suggesting a greater weathering of these profiles and consequently lower clay activity. Despite the sandy texture and lower CEC (15 $\text{cmol}_c \text{ kg}^{-1}$) of Geric Umbric Ferralsol, the total organic carbon contents (Figure 3C) reached 60 g kg^{-1} , and the organic fraction is therefore the main responsible for the charges of the soil. On the other hand, the Hypereutric Katostagnic Gleysol had CEC values that can reach 25 $\text{cmol}_c \text{ kg}^{-1}$ and higher Ki values (Figure 3F). Low SOC values were observed in the profile, and the greatest contribution to the charges of the profile came from high-activity clays.

The highest clay contents were observed for the Ferralsols (Geric Xanthic Ferralsol, Haplic Ferralsol, Geric Ferralsol, and Xanthic Ferralsol; Figure 3D). On the other hand, the Plinthosols, Geric Umbric Ferralsol, and Plinthosols (Amphialbic Katostagnic Plinthosol and Katostagnic Plinthosol) were the ones with the lowest clay contents, followed by Amphialbic ST and Katolixic Ferralsol and Chromic Epiabruptic Lixisol, which showed an

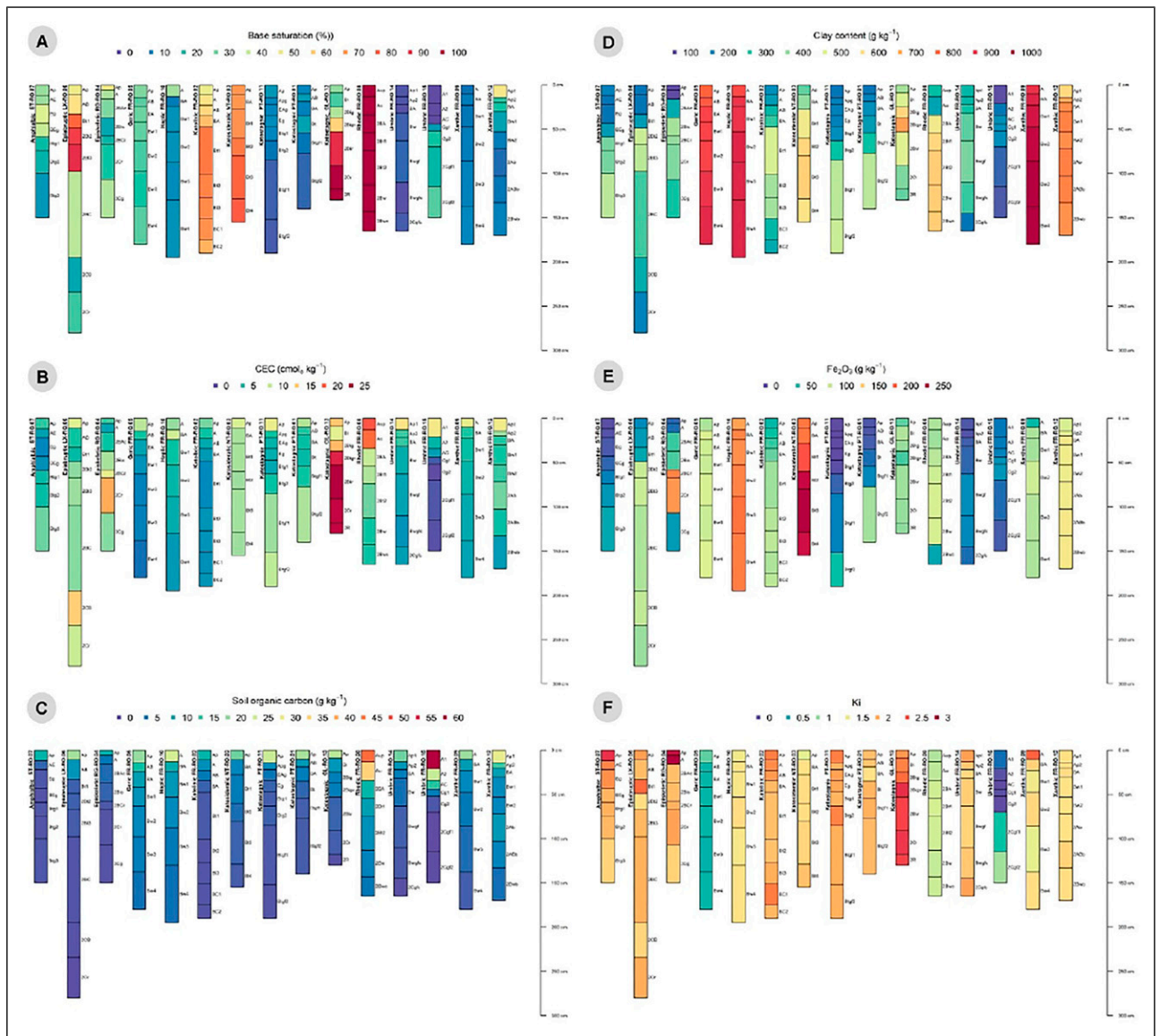


Figure 3. Standardized sketches of the attributes SB (A), CEC (B), SOC (C), clay content (D), iron oxide (E), and Ki index (F) of the horizons of 15 soil profiles of RO, Amazon, Northwestern Brazil.

increase in clay content in subsurface sufficient to characterize the textural gradient²⁶ (Figure 3D).

The highest contents of Fe_2O_3 were observed throughout the profile for Katosideralic NT, followed by Haplic Ferralsol (Figure 3E). On the other hand, the lowest contents of Fe_2O_3 were quantified in the profiles Amphialbic Stagnosol, Amphialbic Katostagnic Plinthosol, Umbric Ferralsol, and Geric Umbric Ferralsol.

The highest Ki values were observed throughout the profile for Hypereutric Katostagnic Gleysol (Figure 3F). On the other hand, Geric Umbric Ferralsol, Geric Ferralsol, and Rhodic FR showed the lowest Ki values. The variations observed are related to the greater or lesser degree of pedogenesis. Ferralsols are more weathered soils, and with this there was greater removal of silica contributing to a decrease in Ki, on the other hand, the conditions in which Gleysol are formed, disfavor weathering, due to the limited removal of products being observed, therefore higher Ki.

The horizontal axis (X) in Figure 4 organizes the differences between the profiles based the Gower distance,⁴⁸

while the vertical component (Y) represents the depths of the horizons according to the field description. The dendrogram scale on the upper left side of Figure 4 corresponds to the numerical dissimilarity in relative (percentage) terms, based on particle-size, chemical, and oxide composition (Table 2).

Thus, Ferralsols with higher clay fraction contents along the profile show greater similarity or likeness in relation to one another, especially the profiles Haplic FR-RO.10, Xanthic FR-RO.12, Xanthic FR-RO.09, and Geric FR-RO.05 (Figure 4).

Next, another cluster was formed between the soils Katostagnic PT-RO.11 and Katostagnic PT-RO.01, which are similar to each other, showing the same contents clay and silt fractions and lower contents of coarse sand fraction. Additionally, Umbric FR-RO.14, Amphialbic ST-RO.07, and Episkeletic RG-RO.04 are also grouped. On the other hand, Umbric FR-RO.15, with lower clay fraction content and the lowest Ki values along the profile, was isolated from the other profiles.

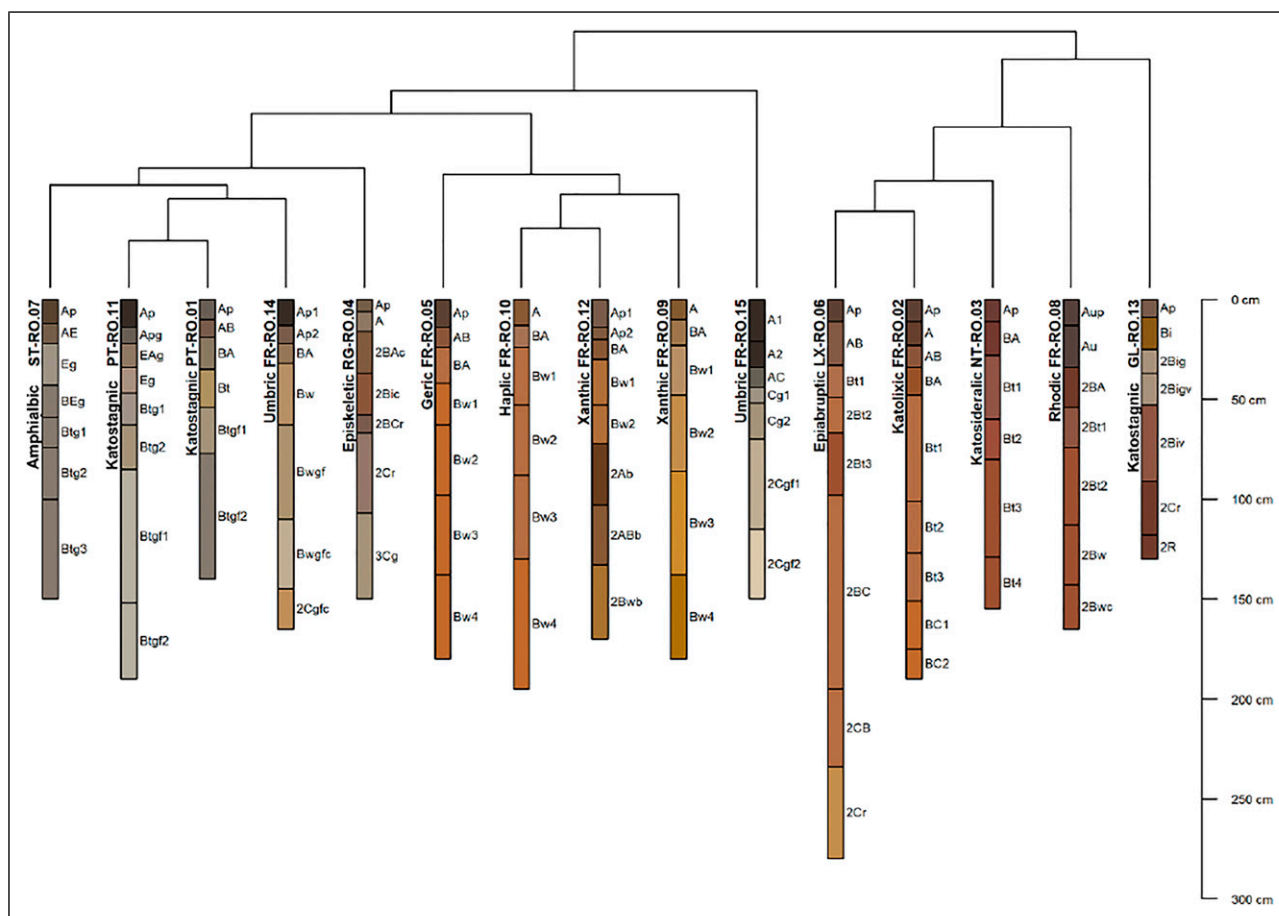


Figure 4. Soil profiles of the State of Rondônia, Brazil, arranged according to the distance of dissimilarity and grouped by the hierarchical clustering method. The dissimilarity values were based on physical attributes, chemical attributes, and oxides (chemical composition of important clay mineral groups).

In opposition, another cluster was formed by the soils Epiabruptic LX-RO.06 and Katolixic FR-RO.02, followed by Katosideralic NT-RO.03, Rhodic FR-RO.08 with higher values of SB and pH along the profile and high values of CEC, K^+ , $Ca^{2+}+Mg^{2+}$, and P in surface. These were followed by Katostagnic GL-RO.13 with high values of SB, pH, CEC, K^+ , $Ca^{2+}+Mg^{2+}$, and P in subsurface and the highest values of Na^+ and Ki along the profile (Figure 4). The total depth of the horizon as a function of the data collected in the field influences the calculation of the dissimilarity between profiles,^{9,10} bearing in mind that in soils with less total depth, the absence of data in deeper layers does not allow their comparison with high depth soils. This can be observed in the dendrogram before the grouping of soils that are sometimes taxonomically distinct.

The pedometric tools allowed a quantitative comparative analysis between soil profiles of the state of Rondônia, supported by morphological characteristics, as observed in the dissimilarity dendrogram (Figure 4). However, more research is needed to better understand the variability of soil properties in subsurface.¹⁰

Spectral behavior of soil profiles

Changes in the physical, chemical, and mineralogical properties of the soil affect its spectral curve, with effects on the (i) intensity of reflectance of the spectrum as a whole

(albedo), (ii) intensity and amplitude of absorption features, and (iii) shape of the spectrum.⁴⁹ The main spectral features observed in the profiles evaluated in this study are schematically presented in Figure 5. The following features are observed: of iron oxides and hydroxides (Fe)-OH at 425, 480, 513, 650, 903, and 1000 nm (from one to six in Figure 5); of hydroxyl groups (O-H) close to 1400 and 1900 nm (7 and 8), which are related to residual water and/or structure 1:1 and 2:1 minerals; of aluminol (Al)-OH groups at 2205 nm (9), present in kaolinite and in some 2:1 minerals; of aluminol groups related to the presence of gibbsite at 2260 nm (10); and subtle features of aluminol groups at 2355 and 2448 nm (11 and 12), mainly related to mica,^{38,50} present in ten of the studied soils.⁵¹ Changes in the shape of the spectrum are also commonly observed, caused by the smoothing of the features due to the presence of organic matter,^{39,52} clearly observed in Figure 5 when comparing the spectra of the surface and subsurface horizons of Katostagnic.

The albedo variation indicates changes in the scattering of reflected energy and is closely related to the particle-size characteristics of the soil.⁵³ Spectra with greater scattering, and consequently greater albedo, are related to sandy textures. The inverse behavior is characteristic of more clayey textures. This pattern is clear in soil profiles with contrasting texture. For example, the profiles Geric FR-RO.05 and Haplic FR-RO.10, with clay content greater than

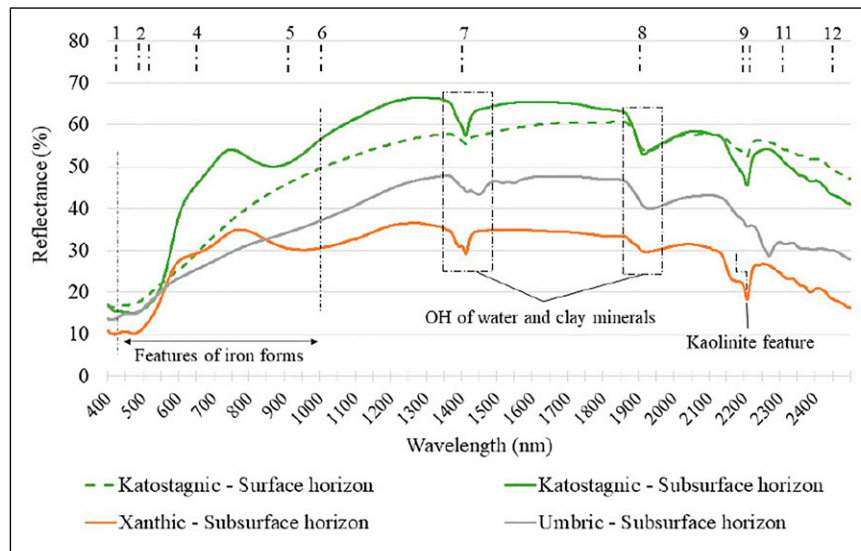


Figure 5. Spectral vis-NIR behavior of some horizons showing the main features observed in the descriptive analysis of the spectra. The features were enumerated to assist their identification in the discussion of the text.

800 g kg⁻¹ in all horizons (Figure 3D), showed maximum reflectance intensity ranging from 40 to 50%. In turn, the profiles Umbric FR-RO.14 and Umbric FR-RO.15, with clay content between 100 and 400 g kg⁻¹, showed maximum reflectance intensity ranging from 60 to 70%. Considering horizons of the same profile, these albedo oscillations are smoother. In this case, texture oscillations can also be more pronounced in the final region of the NIR range (e.g., 2495 nm).^{24,31} These relationships make it possible to infer about the presence of textural gradient between horizons. The profiles Katostagnic PT-RO.01, Katosideralic NT-RO.03, Epiabruptic LX-RO.06, Amphialbic ST-RO.07, and Katostagnic PT-RO.11 showed a significant increase in clay content in subsurface (Figure 3D), and all of them showed reduction of albedo in spectra of subsurface horizons (Figure 6).

Another spectral characteristic of sandy soils is the shape of the curve with positive upward trend, compared to the horizontal shape of curves of clay soils.⁴⁹ This behavior is evident in the Rhodic FR-RO.08 profile (Figure 6O), in which the surface horizons Aup and Au, with clay content around 300 g kg⁻¹, showed a more upward shape and with higher reflectance intensities from 1250 nm when compared with the spectra of the subsurface horizons (2Ba, 2Bt1, 2Bt2, 2Bw, and 2wcB), with clay contents greater than 500 g kg⁻¹. In turn, the textural differentiation observed in Rhodic FR-RO.08 is probably related to lithic discontinuity and not to the action of pedogenesis²⁶.

The smoothing of Fe oxide features due to the presence of organic matter in the surface horizons was observed for all 15 profiles evaluated. This effect is evident in the profiles Rhodic FR-RO.08 (Figure 6O), Katolixic FR-RO.02 (Figure 6M), and Epiabruptic LX-RO.06 (Figure 6N), and occurs less significantly as the SOC gradient decreases, that is, a subtle effect on Haplic FR-RO.10 (Figure 6H) and Xanthic FR-RO.12 (Figure 6I). Figure 6 also shows that the influence of organic components is quite significant in curves of soils with umbric surface horizon (Umbric FR-RO.14 and Umbric FR-RO.15) and pretic surface horizon

(Rhodic FR-RO.08). This highlight is due to the considerable contrast between the organic matter contents of the different horizons, in which the SOC contents ranged from >40 g kg⁻¹ in the surface horizons to values close to 0 g kg⁻¹ in the subsurface horizons (Figure 3C). In the Umbric FR-RO.15 profile, which showed greater contrast of SOC between horizons (>50 g kg⁻¹), the influence of the organic components of surface horizons was so high that they reduced the absorption intensity of virtually all spectral features present (e.g., features of 1:1 and 2:1 clay minerals at 1400, 1900, and 2200 nm). This behavior is typical in soils with high presence of organic materials, so that its masking effect reduces the intensity, slope, and intensity of absorption features in the entire spectrum.⁵³ This behavior is similar to that observed in soil weathering processes, in which low albedo and absorption features with reduced intensity are also observed, which may generate skewed interpretations.⁵⁴

The soils with high Fe₂O₃ contents (Figure 3E) were the ones that showed a more pronounced Fe oxide feature at 900 nm (Figure 6), such as the Ferralsols (Xanthic FR-RO.09, Haplic FR-RO.10, Xanthic FR-RO.12, Geric FR-RO.05, and Katolixic FR-RO.02), Nitisol (Katosideralic NT-RO.03), and the subsurface horizons of Lixisol (Epiabruptic LX-RO.06). This is a spectral characteristic that may be associated with soils with higher pedogenetic evolution and the high degree of crystallinity of iron oxides.^{39,55} Additionally, the narrow convexity of Fe oxide between 450 and 480 nm, observed in almost all soils (Figure 6), is typical of the predominance of goethite over hematite,²⁰ corroborating the predominance of yellowish colors of the studied soils. In this same band, a wider convexity is observed for the profiles Katosideralic NT-RO.03 and Rhodic FR-RO.08, indicating the predominance of hematite,²⁰ which in turn corroborates the reddish colors of the soils of these profiles.

In Ferralsols (Xanthic FR-RO.09, Haplic FR-RO.10, Xanthic FR-RO.12, Geric FR-RO.05, and Katolixic FR-RO.02), the Fe oxide feature is associated with a low

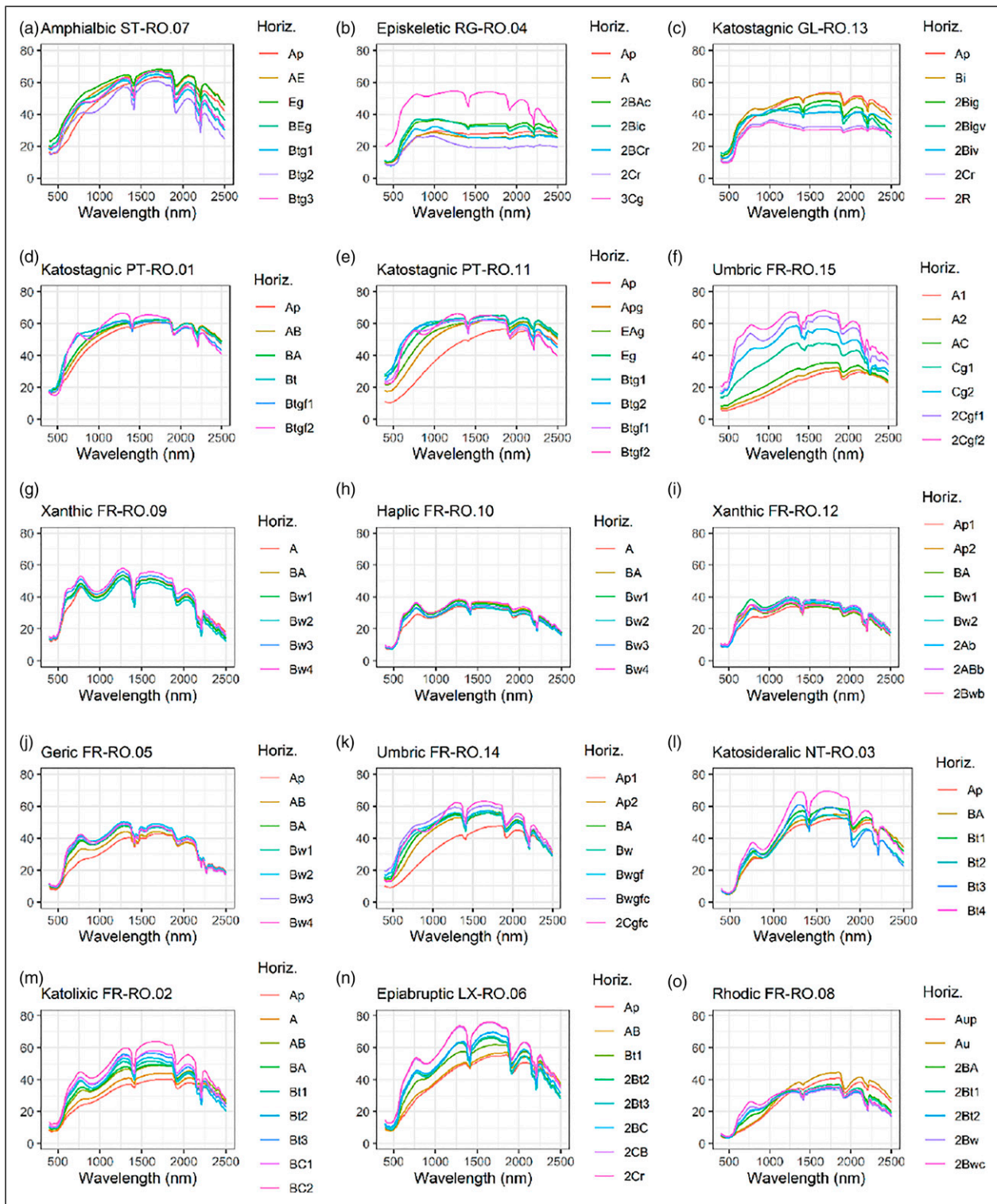


Figure 6. Reflectance of the vis-NIR spectra of samples from each horizon of the respective soil profiles of the State of Rondônia, Brazil. The Y-axes of the graphs were presented in percentage of reflectance.

albedo, rectilinear aspect of the curve up to approximately 2000 nm and downward aspect between 2000 and 2500 nm, spectral characteristics typical of soils of very clayey texture with absence of quartz minerals.²⁰ Moreover, the spectral behavior of these soils is very similar in subsurface, indicating little textural and mineralogical difference between horizons.⁵⁶ The only exception is observed for Katolixic FR-RO.02, which has a greater spectral variation in subsurface, related to the slight textural gradient due to the

presence of Bt horizons. The association between Fe oxide features, spectral aspects of clay soils, and the spectral similarity of the curves of the different profiles confer spectral characteristics typical of a profile with high pedogenetic evolution.²⁹

The soils that were observed poor drainage conditions (Stagnosol RO.07, Katostagnic PT-RO.01, Katostagnic PT-RO.11, Umbric FR-RO.14, and Umbric FR-RO.15) have very low values of Fe₂O₃, as observed in Figure 4B. This

characteristic is due to the environment that favors the reduction and loss of iron and is remarkable in the spectral response of these horizons, with changes in all features of Fe oxides between 425 and 1000 nm. The absence of iron leaves this region with a more linear aspect, without the presence of its characteristic features, especially the absorption with a “shoulder”-like aspect at 650 nm and the concavity at 900 nm. In these profiles (Figure 6), horizons close to the parent material, typically less weathered, start showing again iron features and absorption features of 1:1 and 2:1 minerals (e.g., 1400, 1900, 2200, and 2350 nm), as well as a higher intensity of albedo (Katostagnic PT-RO.01, Katostagnic PT-RO.11, Umbric FR-RO.15, and Rhodic FR-RO.08).

The profiles Katostagnic GL-RO.13 and Episkeletic RG-RO.04 show spectral behavior with very contrasting intensity and shape at different depths (Figure 6). In Episkeletic RG-RO.04 soil, the discordant behavior is observed in the spectrum of the 2BCr and 2Cr horizons, which showed an abrupt reduction of intensity, and the 3Cg horizon, which had higher albedo and clearly more nitid features that were not observed in the surface horizons. In turn, in Katostagnic GL-RO.13, the 2Cr and 2R horizons are the most contrasting in this profile, also due to its abrupt reduction of intensity, rectilinear aspect, and reduction of spectral features that were observed in the spectra of the surface horizons. In both profiles, the discordant characteristic of these spectra reflect significant changes in soil characteristics, signaling the presence of layers of deposition of material from other relief positions.

In summary, the vis-NIR spectral evaluation in subsurface, analyzing different horizons of the same profile, allowed the qualitative characterization of mineralogical components and pedogenetic processes of the different soil profiles. The following characterizations are highlighted: (i) profiles in flooded environments with reduced Fe oxide contents, followed by spectral behaviors characteristic of the parent material in deep horizons; (ii) profiles with similar spectral response throughout its length and presence of iron oxide features, which characterize deep and highly weathered soils, typical of Ferralsols; (iii) profiles with lithological discontinuity with deposition of parent materials of different natures, marked by spectral behavior with very contrasting intensity and shape at different depths; and (iv) textural changes along the profile, typical of Lixisols. These inferences obtained *via* vis-NIR sensors can provide guidance for a probable soil classification. In cases in which indicating the probable soil classification is not possible, the vis-NIR system could at least point out the complexity of pedogenetic processes occurring in such soil profile, requiring a detailed look of the pedologist.

Thus, the results obtained in this study make it possible to assume that the use of vis-NIR spectroscopy, opportunely associated with pedological algorithms,⁵⁷ has great potential to discriminate different soil classes and assist pedologists in surveys in southwestern Amazon. Pedological algorithms might enable automated analysis of vis-NIR data, which in turn allows to increase the sampling density of characterized profiles without making data analysis more difficult.^{20,38} It is also worth pointing out that the instrumentation of penetrometers with vis-NIR sensors that allow characterization in subsurface, offering spectral

response of profiles in operations directly in the field, is recent.^{58,59} The availability of these tools can be extremely useful for more accurate detailed mappings, even in regions with complex characteristics of pedoenvironments, as explored in the present study.

Conclusion

The functionalities of the AQP package (e.g., graphical plots showing the variations of attributes' concentrations and the colors of soil horizons in-depth) allowed to visualize the variations of physical, chemical, and oxide attributes of the different profiles. In addition, the similarity analysis (clustering analysis) of the AQP package applied to the soil profiles grouped the most clayey Ferralsols and soils formed in poorly drained environments, especially Plinthosols and Stagnosol. These inferences made in a fast and automated way via the AQP package allow a synoptic view of the data set by the pedologist, simplifying his work of classifying the soil profiles.

The evaluation of spectral characteristics in-depth allows inferring about pedogenetic processes (e.g., textural changes along the profile, profiles in flooded environments with reduced contents of Fe oxide, profiles with similar spectral response throughout their extension, and profiles with lithological discontinuity). In this sense, our results showed that the inferences obtained *via* spectral data can complement those obtained with the AQP package, as they allowed for insights into the classification of soils in a region with a complex diversity of pedoenvironments. The recent technological advances that enabled in-situ operations using vis-NIR spectrometers for soil profile evaluations should encourage future studies to evaluate the association of vis-NIR spectroscopy with pedological algorithms (e.g., AQP package) in order to create pedometric tools for simplifying soil surveys.

Declaration of Conflicting Interests

The authors declared no potential conflicts of interest with respect to the research, authorship, and/or publication of this article.

Funding

The authors received no financial support for the research, authorship, and/or publication of this article.

ORCID iD

Marcos G Pereira  <https://orcid.org/0000-0002-1402-3612>

References

1. Silveira ALP and Paixão KRC. Vegetação do estado de Rondônia. In: JF Lumbreras, LM Silva, LHC Anjos, et al (eds) *Delarmelinda-Honoré EA, Burity KTL. Guia de campo da XII Reunião Brasileira de Classificação e Correlação de Solos: RCC de Rondônia*. Embrapa: Embrapa Solos-Livro técnico (INFOTECA-E); 2019.
2. Fernandes LC and Guimarães SCP. *Atlas geoambiental de Rondônia*. 2nd ed. Porto Velho. Secretaria de Estado do Desenvolvimento Ambiental; 2002.
3. RONDÔNIA. Secretaria de Estado do Planejamento e Coordenação Geral. *Diagnóstico Socioeconômico-Ecológico do Estado de Rondônia e assistência técnica para formulação*

- da segunda aproximação do Zoneamento Socioeconômico-Ecológico. Rio de Janeiro: Tecnosolo/DHV Consultants/Eptisa, 1998, pp. 157.
4. Dantas ME and Adamy A. Compartimentação do relevo do Estado de Rondônia. In: A Adamy (ed) *Geodiversidade do Estado de Rondônia*. Porto Velho: CPRM; 2010, pp. 37–54.
 5. Oliveira VA, Lumbreras JF, Coelho MR, et al. Solos da XII reunião brasileira de classificação e correlação de solos: RCC de Rondônia. In: Lumbreras JF, Silva LM, Anjos LHC, et al. (eds) *Delarmelinda-Honoré EA, Burity KTL. Guia de campo da XII Reunião Brasileira de Classificação e Correlação de Solos: RCC de Rondônia*. Rondônia: Embrapa Solos-Livro técnico (INFOTECA-E); 2019.
 6. Schlindwein JA, Marcolan AL, Fioreli-Perira EC, et al. Solos de Rondônia: Usos e perspectivas. *Revista Brasileira de Ciências da Amazônia* 2012; 1(1): 213–231.
 7. Shinzato E, Teixeira WG and Mendes AM. Solos de Rondônia. In: A. Adamy (eds) *Geodiversidade do Estado de Rondônia*. Porto Velho: CPRM; 2010, pp. 56–78.
 8. Roudier P and Beaudette D. Visualisation and modelling of soil data using the aqp package. In: The R User Conference, useR!, University of Warwick. Coventry, UK. University of Warwick; 2011, pp. 92.
 9. Beaudette DE, Roudier P and O'Geen AT. Algorithms for quantitative pedology: a toolkit for soil scientists. *Comput Geosci* 2013; 52: 258–268, DOI: [10.1016/j.cageo.2012.10.020](https://doi.org/10.1016/j.cageo.2012.10.020).
 10. Pinheiro HSK, de Carvalho W, da Silva Chagas C, et al. Using soil depth functions to distinguish dystric from xanthic ferralsols in the landscape. In: AE Hartemink and B Minasny (eds) *Digital Soil Morphometrics*. Cham: Springer; 2016b, pp. 295–313.
 11. Pinheiro HSK, dos Anjos LHC, Xavier PA, et al. Quantitative pedology to evaluate a soil profile collection from the Brazilian semi-arid region. *South Afr J Plant Soil* 2018; 35(4): 269–279, DOI: [10.1080/02571862.2017.1419385](https://doi.org/10.1080/02571862.2017.1419385)
 12. Viscarra Rossel RA, Behrens T, Ben-Dor E, et al. A global spectral library to characterize the world's soil. *Earth-Sci Rev* 2016; 155: 198–230, DOI: [10.1016/j.earscirev.2016.01.012](https://doi.org/10.1016/j.earscirev.2016.01.012)
 13. Chabrilat S, Gholizadeh A, Neumann C, et al. Preparing a soil spectral library using the internal soil standard (ISS) method: influence of extreme different humidity laboratory conditions. *Geoderma* 2019; 355: 113855, DOI: [10.1016/j.geoderma.2019.07.013](https://doi.org/10.1016/j.geoderma.2019.07.013)
 14. Demattê JAM, Dotto AC, Paiva AF, et al. The Brazilian soil spectral library (BSSL): a general view, application and challenges. *Geoderma* 2019; 354: 113793, DOI: [10.1016/j.geoderma.2019.05.043](https://doi.org/10.1016/j.geoderma.2019.05.043)
 15. Seidel M, Hutengs C, Ludwig B, et al. Strategies for the efficient estimation of soil organic carbon at the field scale with vis-NIR spectroscopy: spectral libraries and spiking vs local calibrations. *Geoderma* 2019; 354: 113856, DOI: [10.1016/j.geoderma.2019.07.014](https://doi.org/10.1016/j.geoderma.2019.07.014)
 16. Stenberg B, Rossel RAV, Mouazen AM, et al. Visible and near infrared spectroscopy in soil science. *Adv Agron* 2010; 107: 163–215, DOI: [10.1016/S0065-2113\(10\)07005-7](https://doi.org/10.1016/S0065-2113(10)07005-7)
 17. Asgari N, Ayoubi S, Jafari A, et al. Incorporating environmental variables, remote and proximal sensing data for digital soil mapping of USDA soil great groups. *Int J Remote Sensing* 2020a; 41(19): 7624–7648, DOI: [10.1080/01431161.2020.1763506](https://doi.org/10.1080/01431161.2020.1763506)
 18. Asgari N, Ayoubi S, Demattê JAM, et al. Digital mapping of soil drainage using remote sensing, DEM and soil color in a semiarid region of Central Iran. *Geoderma Reg* 2020b; 22: e00302, DOI: [10.1016/j.geodrs.2020.e00302](https://doi.org/10.1016/j.geodrs.2020.e00302)
 19. Asgari N, Ayoubi S, Demattê JAM, et al. Carbonates and organic matter in soils characterized by reflected energy from 350–25000 nm wavelength. *J Mountain Sci* 2020c; 17(7): 1636–1651, DOI: [10.1007/s11629-019-5789-9](https://doi.org/10.1007/s11629-019-5789-9)
 20. Demattê JAM and Terra FS. Spectral pedology: a new perspective on evaluation of soils along pedogenetic alterations. *Geoderma* 2014; 217: 190–200, DOI: [10.1016/j.geoderma.2013.11.012](https://doi.org/10.1016/j.geoderma.2013.11.012)
 21. Moura-Bueno JM, Dalmolin RSD, ten Caten A, et al. Stratification of a local VIS-NIR-SWIR spectral library by homogeneity criteria yields more accurate soil organic carbon predictions. *Geoderma* 2019; 337: 565–581, DOI: [10.1016/j.geoderma.2018.10.015](https://doi.org/10.1016/j.geoderma.2018.10.015)
 22. Coblinski JA, Giasson É, Demattê JAM, et al. Prediction of soil texture classes through different wavelength regions of reflectance spectroscopy at various soil depths. *Catena* 2020; 189: 104485, DOI: [10.1016/j.catena.2020.104485](https://doi.org/10.1016/j.catena.2020.104485)
 23. Ramos PV, Inda AV, Barrón V, et al. Color in subtropical Brazilian soils as determined with a Munsell chart and by diffuse reflectance spectroscopy. *Catena* 2020; 193: 104609, DOI: [10.1016/j.catena.2020.104609](https://doi.org/10.1016/j.catena.2020.104609)
 24. Souza AB, Demattê JAM, Mello FA, et al. Ratio of clay spectroscopic indices and its approach on soil morphometry. *Geoderma* 2020; 357: 113963, DOI: [10.1016/j.geoderma.2019.113963](https://doi.org/10.1016/j.geoderma.2019.113963)
 25. IUSS Working Group WRB. *World Reference Base for Soil Resources 2014, Update 2015 International Soil Classification System for Naming Soils and Creating Legends for Soil Maps*. Rome: World Soil Resources Reports/FAO, 2015.
 26. Santos HG, Jacomine PKT, Anjos LHC, et al. *Sistema Brasileiro de Classificação de Solos*. Brasília: Embrapa, 2018.
 27. Rizzo R, Demattê JAM and Terra FDS. Using numerical classification of profiles based on Vis-NIR spectra to distinguish soils from the Piracicaba Region, Brazil. *Revista Brasileira de Ciência do Solo* 2014; 38(2): 372–385, DOI: [10.1590/S0100-06832014000200002](https://doi.org/10.1590/S0100-06832014000200002)
 28. Vasques GM, Demattê JAM, Viscarra Rossel RAV, et al. Soil classification using visible/near-infrared diffuse reflectance spectra from multiple depths. *Geoderma* 2014; 223: 73–78, DOI: [10.1016/j.geoderma.2014.01.019](https://doi.org/10.1016/j.geoderma.2014.01.019)
 29. Terra FS, Demattê JAM and Viscarra Rossel RA. Proximal spectral sensing in pedological assessments: vis-NIR spectra for soil classification based on weathering and pedogenesis. *Geoderma* 2018; 318: 123–136, DOI: [10.1016/j.geoderma.2017.10.053](https://doi.org/10.1016/j.geoderma.2017.10.053)
 30. Di Iorio E, Circelli L, Lorenzetti R, et al. Estimation of andic properties from Vis-NIR diffuse reflectance spectroscopy for volcanic soil classification. *Catena* 2019; 182: 104109, DOI: [10.1016/j.catena.2019.104109](https://doi.org/10.1016/j.catena.2019.104109)
 31. Marques KP, Rizzo R, Dotto AC, et al. How qualitative spectral information can improve soil profile classification? *J Near Infrared Spectrosc* 2019; 27(2): 156–174, DOI: [10.1177/0967033518821965](https://doi.org/10.1177/0967033518821965)
 32. Lumbreras JF, da Silva LM, dos Anjos LHC, et al. *Guia de campo da XII Reunião Brasileira de Classificação e Correlação de Solos: RCC de Rondônia*. Brasília: Embrapa, 2019

33. EMBRAPA - Empresa Brasileira DE Pesquisa Agropecuária. *Centro Nacional de Pesquisa de Solos*. Rio de Janeiro: Manual de métodos de análise de solo, 1997, p. 212.
34. Nelson DW and Sommers LE. Total carbon, organic carbon, and organic matter. In: DL Sparks (ed) *Methods of soil analysis, Part 3 – Chemical methods*. Madison: American Society of Agronomy Soil Science Society of America; 1996, p. 1264.
35. Teixeira PC, Donagemma GK, Fontana A, et al. *Manual de métodos de análise de solo*. Brasília: Embrapa, 2017.
36. R Development Core Team. *R: A Language and Environment for Statistical Computing*. Vienna: R Foundation for Statistical Computing, 2019.
37. Terra FS, Demattê JAM and Viscarra Rossel RA. Spectral libraries for quantitative analyses of tropical Brazilian soils: Comparing vis-NIR and mid-IR reflectance data. *Geoderma* 2015; 255: 81–93, DOI: [10.1016/j.geoderma.2015.04.017](https://doi.org/10.1016/j.geoderma.2015.04.017)
38. Demattê JAM, Campos RC, Alves MC, et al. Visible-NIR reflectance: a new approach on soil evaluation. *Geoderma* 2004; 121(1–2): 95–112, DOI: [10.1016/j.geoderma.2003.09.012](https://doi.org/10.1016/j.geoderma.2003.09.012)
39. Ponce-Hernandez R, Marriott FHC and Beckett PHT. An improved method for reconstructing a soil-profile from analysis of a small number of samples. *J Soil Sci* 1986; 37: 455–467, DOI: [10.1111/j.1365-2389.1986.tb00377.x](https://doi.org/10.1111/j.1365-2389.1986.tb00377.x)
40. Malone BP, McBratney AB and Minasny B. Empirical estimates of uncertainty for mapping continuous depth functions of soil attributes. *Geoderma* 2011; 160: 614–626, DOI: [10.1016/j.geoderma.2010.11.013](https://doi.org/10.1016/j.geoderma.2010.11.013)
41. Pinheiro HSK, Xavier PAM, Anjos LHC, et al. Pedometric tools applied to zoning management of areas in brazilian semiarid region. In: Moudrý J, Bernas J, Mendes KF, et al. (eds). *Multifunctionality and Impacts of Organic and Conventional Agriculture*. London, UK: IntechOpen; 2019. DOI: [10.5772/intechopen.88526](https://doi.org/10.5772/intechopen.88526)
42. Pinheiro HSK, da Silva Chagas C, de Carvalho Júnior W, et al. Ferramentas de pedometria para caracterização da composição granulométrica de perfis de solos hidromórficos. *Pesquisa Agropecuária Brasileira* 2016a; 51(9): 1326–1338, DOI: [10.1590/s0100-204x2016000900032](https://doi.org/10.1590/s0100-204x2016000900032)
43. Prado RDM and Centurion JF. Alterações na cor e no grau de flocculação de um Latossolo Vermelho-Escuro sob cultivo contínuo de cana-de-açúcar. *Pesquisa Agropecuária Brasileira* 2001; 36: 197–203
44. Oades JM. The retentions of organic matter in soils. *Biogeochemistry* 1988; 5: 35–70.
45. Gomes PC, Moura Filho W, Costa LM, et al. Influência da cobertura vegetal na formação e evolução de húmus e sua relação com grau de flocculação de um latossolo vermelho-amarelo do município de viçosa, minas gerais. *Revista Ceres* 1994; 41235: 223–233.
46. Cavassani RDS, Anjos LHCD, Pereira MG, et al. Amazonian dark earths in Rondônia state: soil properties, carbon dating and classification. *Revista Brasileira de Ciência do Solo* 2021; 45: e0200160, DOI: [10.36783/18069657rbc20200160](https://doi.org/10.36783/18069657rbc20200160)
47. Minasny B, Stockmann U, Hartemink AE, et al. Measuring and modelling soil depth functions. In: Hartemink AE and Minasny B (eds) *Digital Soil Morphometrics*. Cham: Springer; 2016, pp. 225–240.
48. Gower JC. A general coefficient of similarity and some of its properties. *Biometrics* 1971; 27: 857–871.
49. Demattê JAM. Characterization and discrimination of soils by their reflected electromagnetic energy. *Pesquisa Agropecuária Brasileira* 2002; 37(10): 1445–1458, DOI: [10.1590/S0100-204X2002001000013](https://doi.org/10.1590/S0100-204X2002001000013)
50. Bowers SA and Hanks JR. Reflection of radiant energy from soil. *Soil Sci* 1965; 100: 130–138.
51. Calderano SB, Oliveira AP and Gregoris G. Mineralogia da fração argila dos solos da XII Reunião Brasileira de Classificação e Correlação de Solos – estado de Rondônia. In: Lumberas JF, da Silva LM, dos Anjos LHC, et al. (eds) *Wadt PGS, Pereira MG, Delarmelinda-Honoré EA, Burity KTL. Guia de campo da XII Reunião Brasileira de Classificação e Correlação de Solos: RCC de Rondônia*. Brasília: Embrapa; 2019.
52. Bellinaso H, Demattê JAM and Romeiro SA. Soil spectral library and its use in soil classification. *Revista Brasileira de Ciência do Solo* 2010; 34(3): 861–870, DOI: [10.1590/S0100-06832010000300027](https://doi.org/10.1590/S0100-06832010000300027)
53. Ben-Dor E. Quantitative remote sensing of soil properties. *Adv Agron* 2002; 75: 173–244, DOI: [10.1016/S0065-2113\(02\)75005-0](https://doi.org/10.1016/S0065-2113(02)75005-0)
54. Ben-Dor E, Inbar Y and Chen Y. The reflectance spectra of organic matter in the visible near infrared and short-wave infrared region (400–2500 nm) during a control decomposition process. *Rem Sens Env* 1997; 61: 1–15, DOI: [10.1016/S0034-4257\(96\)00120-4](https://doi.org/10.1016/S0034-4257(96)00120-4)
55. Benedet L, Faria WM, Silva SHG, et al. Soil subgroup prediction via portable X-ray fluorescence and visible near-infrared spectroscopy. *Geoderma* 2020; 365: 114212, DOI: [10.1016/j.geoderma.2020.114212](https://doi.org/10.1016/j.geoderma.2020.114212)
56. Demattê JAM, Bellinaso H, Romero DJ, et al. Morphological interpretation of reflectance spectrum (MIRS) using libraries looking towards soil classification. *Scientia Agricola* 2014; 71(6): 509–520, DOI: [10.1590/0103-9016-2013-0365](https://doi.org/10.1590/0103-9016-2013-0365)
57. Rossiter DG. Past, present & future of information technology in pedometrics. *Geoderma* 2018; 324: 131–137, DOI: [10.1016/j.geoderma.2018.03.009](https://doi.org/10.1016/j.geoderma.2018.03.009)
58. Ackerson JP, Morgan CLS and Ge Y. Penetrometer-mounted visNIR spectroscopy: application of EPO-PLS to *in situ* VisNIR spectra. *Geoderma* 2017; 286: 131–138, DOI: [10.1016/j.geoderma.2016.10.018](https://doi.org/10.1016/j.geoderma.2016.10.018)
59. Pei X, Sudduth KA, Veum KS, et al. Improving *in-situ* estimation of soil profile properties using a multi-sensor probe. *Sensors* 2019; 19(5): 1011, DOI: [10.3390/s19051011](https://doi.org/10.3390/s19051011)